Study of the Mechanical-Photoacoustic Properties of Thermally Modified Al-6061-T6

B. Gonzalez-Vizcarra[a], I. A. Figueroa[b], *, O. Novelo-Peralta[b], A. Delgado-Hernández[a],
M. Siqueiros-Hernández[c], R. Castañeda-Guzmán[d], and C. G. Díaz[e]

[a] *Faculty of Engineering Sciences and Technology, Universidad Autónoma de Baja California,*
Blvd. Universitario #1000, Unidad Valle de las Palmas. Tijuana, Baja California, C.P. 2150018 México

[b] *Institute of Materials Reserach, Universidad Nacional Autónoma de México, Circuito Exterior S/N,*
Circuito de la Investigación Científica, Ciudad Universitaria, C.P. 04510 Cd. México

[c] *Faculty of Engineering, Universidad Autónoma de Baja California,*
Blvd. Benito Juárez s/n Col: Ex Ejido Coahuila, Mexicali, Baja California, C.P. 21280 México

[d] *Institute of Applied Science and Technology, Universidad Nacional Autónoma de México, Circuito Exterior S/N,*
Circuito de la Investigación Científica, Ciudad Universitaria, C.P. 04510 Cd. México

[e] *Faculty of Chemical Sciences and Engineering, Universidad Autónoma de Baja California,*
Calzada Universidad #14418, Parque Industrial Internacional Tijuana, Baja California, C.P. 22390 México
*e-mail: iafigueroa@unam.mx

Abstract—This study consists of a series of heat treatments (solubilization and aging) and a cold work process on Al 6061-T6 samples, in order to study the effect of temperature and mechanical properties through tensile, hardness and photoacoustic tests. The cold-worked and 200°C aged sample showed the highest values for yield strength, ultimate tensile strength and fracture strength. For the sample heat treated at 150°C, the values obtained for plasticity (58.29 kJ/m^3) and toughness (56.95 kJ/m^3) were the highest. The age hardening treatment at 200°C for 1 h reached the maximum precipitation hardening, similar to the T6 condition. The changes observed in the photoacoustic signal were correlated with the phase transformations detected by DSC thermograms, being first peak (Zone I) associated to the formation of vacancy-silicon clusters. The second peak (Zone II) to the formation of GP-I zones and needle-like GP-II zones or/β". The third peak (Zone III) to the formation of rod-like β'-phase. The photoacoustic analyses proved to be rather useful when measuring the microestructural changes in Al alloys. Finally, the results reported here, favors the use of this material in components with high levels of manufacturing/machining to produce complex geometries.

INTRODUCTION

Aluminum (Al) is the preferred material for light components in the automotive and aerospace industries thanks to its high strength/weight ratio, excellent wear resistance and high working temperatures, mechanical properties, or a combination of all of these [1]. Currently, almost two-thirds of all extruded products are made of Al, and 90% of these are fabricated with 6061 alloys, which include Magnesium−Silicon (Al−Mg−Si) [1−4].

Heat treatments consist of heating up and keeping the material in adequate conditions. The main parameters for heat treatments are time and temperature, this with the aim of obtaining the desired characteristics or proprieties in the alloy. In the specific case of the Al-6061 alloy, when the material is put through heat treatment or thermomechanical processing, its mechanical properties reach the highest values, becoming a mechanically enhanced material, especially when compared to other Al alloys [5, 6].

Nowadays the case of heat treatable Al 6061 alloy is one of the most relevant, because of its wide range of applications, as numerous studies have been conducted to improve its mechanical properties. Demir [7], reported the effect of artificial aging on the machinability of Al 6061, first at the condition at which it is commercialized, and second after solubilization at 530°C for 4 h, followed by water quenching at room temperature (SHT) and solubilization with artificial aging at 180°C for 4 h, followed by water quenching (SHTA). It was reported that the samples were artificially aged at 180°C for 1, 5, 11, and 24 h, followed by air-cooling. The results showed that the alloy reached its maximum hardness at 180°C when aged for

11 hours. However, the shear strengths were not significantly influenced by the aging treatment, coinciding with the results reported by Bohórquez [3] with similar heat treatment, but for 18 h of aging. Tan et al. [8] concluded that the optimal aging is achieved between 175 and 195°C, with a times of permanence between 2 and 6 h. This proved that the contribution of short aging time is comparable to that of a more prolonged one, allowing energy saving. On the other hand, Brodova et al. reported the structural evolution in quenched Al-based alloys during severe plastic deformation. They found that the increment in tensile strength and hardness was associated with the formation of nanograins [9].

Mansourinejad [10] reported that one single aging process at 180°C, for 4 h, in combination with different deformation percentages, improved the resistance as well as the elongation of the material. This was attributed to the influence of the combination of artificial aging and cold worked upon solubilization at 520°C for 1 h, and the subsequent water quenching. The changes in the mechanical properties were related to the dissolution, growth and coarsening of precipitates. The well-known precipitation sequence for Al−Mg−Si alloys is shown below (1):

$$SSSS \rightarrow GP\ Zones \rightarrow \beta'' \rightarrow \beta \rightarrow \beta(Mg_2Si). \quad (1)$$
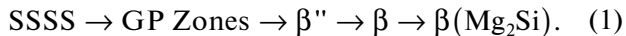
The photoacoustic effect is the generation of sound using modulated light or laser pulses absorbed by a physical system. The acoustic signal is a consequence of a pressured wave traveling in the crystal, induced by the incidence of the laser beam. The mechanically stressed state of the crystal, created by the pressure produced by the wave, activates stresses and strains in the lattice in such way that changes of volume as a function of pressure is expected. In the photoacoustic technique, the temperature dependence of fluctuations of physical properties that couple sufficiently strongly to the crystalline indicatrix can be examined. This is the case for structural phase transitions, such as those occurring in a ferro-paraelectric transition in ceramics [11−16] and metallic alloys [17].

Castañeda and others reported microstructural changes in metallic materials by PLPA (pulsed laser photoacoustic technique) using laser pulses. These changes were associated to the modification of ferroelectric properties [14, 16−24]. Aldebarran and others, associated the phase transformations with the paraelectric behavior of ZnO−ZnS thin films; they also mention that the transformations are presented at low temperature, being of nanometric size [22, 23, 25−27]. On the other hand, Pérez et al., demonstrated through photoacoustic studies to V_2O_5 thin films, phase transformations that modified the surface and optical properties of the thin films [28−30]. Therefore, the objective of this work is to study the effect of temperature and the mechanical properties through tensile, hardness, and photoacoustic tests for the Al 6061 alloy at different heat treatment parameters.

EXPERIMENTAL

A series of heat treatments (solubilization and aging), as well as a cold worked process (CW) were applied to Al 6061-T6 samples (as-received samples). These were carried out in order to assess the effect of temperature and plastic deformation on the mechanical properties of the alloy. The treated samples were put through tensile and hardness tests to determine any change in toughness, ductility, and resistance based on the values of yield strength, ultimate tensile strength (UTS), and fracture strength [31−33]. The homogeneous solid solution was obtained through a solubilization process, while aging was used mainly to improve and stabilize the precipitation of small Al, Mg, or Si phases, which determine the mechanical behavior these alloys.

The heat treatments were carried out with a 6.35 mm thick Al 6061-T6 sheet, a total of 24 rectangular subsize test specimens were machined under the ASTM E8-17 specifications [34]. Twenty test specimens were heat-treated at 555°C for 1 h, followed by a water quenched. The aging process was applied with sets of four test specimens at 150, 175, and 200°C for 1 h, respectively. The aging process ended with the samples quenched in water. The Cold-worked samples were deformed up to 5% before the tensile testing.

The tensile tests were performed using a Shimadzu® universal testing machine with a deformation speed of 0.5 mm/min, following the ASTM E8−17 specifications [34]. The Hardness Tests were carried out with two machines: Wilson Hardness Tukon® 1102 [35] and Shimadzu Twin Mod 123. In both cases, the load applied was 4.9 N and 5 indentations were carried out, as indicated by the ASTM E92−17 [36].

The photoacoustic experimental set-up employed in this work, consisted of a pulsed Nd:YAG laser (Ekspla 3100, with a 5 ns pulse width, and a repetition rate of 10 Hz at a wavelength of 355 nm). A beam splitter and a pyroelectric detector; a commercial electric tube furnace connected to a PID temperature control; and a piezoelectric ceramic coupled to the sample through a quartz bar. The averaged signals (150 scans) were monitored with a digital oscilloscope [11, 12]. The heating speed employed was 3°C/min between 23 and 270°C in the OTF 1200X horizontal tubular furnace. The wavelength readings were registered every 2°C. The outcoming acoustic signal detected by a piezoelectric transducer was generated in the bulk Al alloys, that were adhered to a quartz rod. These experiments were carried out at a slow heating rate in order to consider the experiment as temperature constant events.

RESULTS AND DISCUSSION

Table 1 shows the values for the resilience energy (E_R) plasticity (E_P) and toughness (E_r) obtained in this

Table 1. Stress and strain values, and resilience energy (E_R), plasticity (E_p) and toughness (E_r) of the tested materials. CW = Cold worked

Mechanical properties	As-received sample	Solubilized sample	150°C	150°C/CW	175°C	175°C/CW	200°C	200°C/CW
σ_0, kPa	299	60.8	175	250.5	200	260	299	334
σ_{max}, kPa	315	190	275	299	265	270	315	333
σ_{rup}, kPa	275	150	225	248.5	230	240	260	299
ε_0	0.07	0.02	0.04	0.05	0.07	0.05	0.06	0.07
ε_{max}	0.12	0.27	0.23	0.23	0.13	0.15	0.14	0.07
ε_{rup}	0.16	0.35	0.29	0.26	0.15	0.18	0.18	0.11
E_R, kJ/m^3	9.72	0.61	3.59	6.26	6.50	6.50	8.22	10.86
E_P, kJ/m^3	28.08	50.69	*58.29*	*61.01*	27.16	32.65	35.88	12.46
E_r, kJ/m^3	23.19	50.53	*56.95*	50.84	20.35	30.20	30.36	11.18

Table 2. Average HV_{500} Vickers hardness

As received sample	Solubilized	150°C	150°C/CW	175°C	175°C/CW	200°C	200°C/CW
109 HV_{500}	93 HV_{500}	91 HV_{500}	104 HV_{500}	106 HV_{500}	101 HV_{500}	98 HV_{500}	116 HV_{500}

work. These were calculated using Eqs. (2)–(4), respectively, as well as the values for the yield strength and strain (σ_0, ε_0), UTS and strain (σ_{max}, ε_{max}) and stress and strain at the fracture (σ_{rup}, ε_{rup}) obtained from the σ vs. ε curves.

$$E_{resilience} = \frac{\sigma_0 \varepsilon_0}{2}, \qquad (2)$$

$$E_{Plasticity} = (\sigma_{max}\, \varepsilon_{max}) - E_{resilience}, \qquad (3)$$

$$E_{toughness} = (\sigma_{rup}\, \varepsilon_{rup}) - 2E_{resilience}. \qquad (4)$$

Table 2 shows the resulting HV_{500} hardness average values. The values of the cold-worked test specimens showed the same tendency.

The aforementioned mechanical parameters (Table 1) were determined from the number of σ vs. ε curves generated during the tensile tests for each test specimen. Using these values, the energy necessary to deform the material in the elastic and plastic zones, and its toughness were calculated. These were related to the area under the curve, with resilience, plasticity and toughness, respectively (Table 1). The changes in the microstructure are controlled by the heat treatment conditions, in specific with time and temperature. In this particular case, the heat treatment was performed at different temperatures with the same time of permanence. As the temperature of heat treatment increases, the maximum peak of precipitation is more quickly reached, as can be seen in Table 1.

The cold-worked (CW) and 200°C aged specimen (200°C + CW) shows the highest values for yield strength (334 kPa), UTS (333 kPa), and fracture strength (299 kPa), as well as for resilience (10.86 kJ/m^3). It is important to mention that these values are very similar to those obtained for the as-received sample. Whereas the values obtained for plasticity (58.29 kJ/m^3) and toughness (56.95 kJ/m^3) in the sample heat treated at 150°C were found to be the highest. It is well known that the increment in the tensile strength is accompanied by a decrease in the plasticity and toughness. Thus, the behavior observed in the tested samples was the expected.

As mentioned before, the as received/initial sample was an Al 6061 alloy in T6 condition. The T6 temper provides the maximum precipitation hardening, it consists in solution heat treatment at 530°C for 30 min, then a rapid water quenching followed by an age hardening at 175°C for 8 h. The result indicated that an age hardening treatment at 200°C for 1 h, the samples reached the maximum precipitation hardening, similar to the T6 condition. The same behavior was observed in the Vickers hardness test (Table 2), where the maximum Hv was observed in the sample aged-treated at 200°C, followed by the cold worked. This value is similar to those obtained for the T6 condition sample. The lowest value was obtained for samples treated at 150°C.

For photoacoustic signals analysis, PA(t, $T1$) is the average photoacoustic signal of N signals at a temperature "$T1$". When this procedure is repeated for different temperatures, the functions PA(t, $T2$), PA(t, $T3$), were obtained. It was assumed that the correlation between PA(t, Ti) and PA(t, $Ti + 1$) will reveal the changes that occur in the sample as a function of the experimental temperature. Therefore, the function
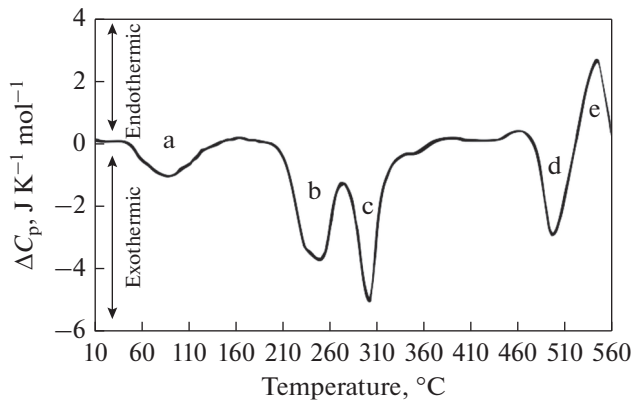
Fig. 1. Acoustic Stability vs. Temperature of solubilized sample at 555°C. Three microstructural changes can be seen: 50, 12, and 25%, respectively. Modified from [37].

Fig. 2. Acoustic Stability vs. Temperature of solubilized sample at 555°C.

$f(T)$ with a maximum correlation value for each temperature (that represents the mean square value) can be built. This function $f(T)$, built through the average photoacoustic signals, contains the behavioral information of the sample as a function of the temperature. The t index indicates the size of the temporal signal. In conclusion, the correlation between the PA (Ti) and PA (Ti + i) signals indicates the range of temperature over which the phase transformations take place.

According to Dutta and Allen [37], the precipitation processes in the Al 6061 alloy can be determined by means of a DSC thermograms (Fig. 1), where the first exothermic event at 82°C (peak a) is associated with the formation of vacancy-silicon clusters, the second exothermic event at 241.85°C (peak b) is an overlapping of two peak associated with the formation of GP-I zones and needle-like GP-II zones or/β" and third exothermic peak at 292°C (peak c) is associated with the formation of rod-like β'-phase. The fourth exothermic peak at 493.85°C (peak d) is related to the formation of plate-shaped β-phase (Mg_2Si). Finally, the endothermic peak at 547°C is associated to the dissolution process.

Figure 2 shows the acoustic stability signal spectrum *vs.* temperature, that was acquired for the Al 6061 alloy sample, solubilized at 550°C for one hour. As can be observed, the first peak that is associated to a change in acoustic signal wavelength appears between 98 and 130°C (Zone I). A second peak in this chart appears in the 130 to 170°C (Zone II) temperature range, with a change of 12%. Finally, a third peak appears between 170 and 220°C, associated to 25% of the transformation (Zone III). Then a stabilization of signal zone is detected.

The changes observed in the photoacoustic signal can be correlated with the phase transformations detected using DSC thermograms, in this sense, the first peak in the acoustic signal wavelength (Zone I) can be as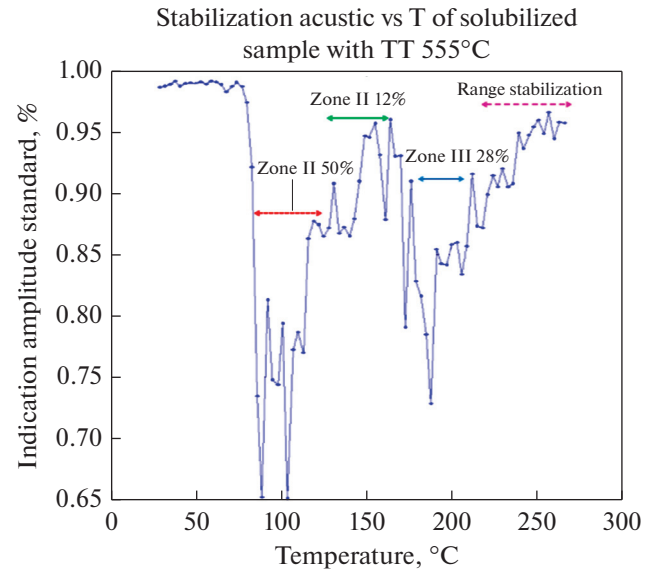sociated to the formation of vacancy-silicon clusters. The second peak (Zone II) could be related to the formation of GP-I zones and needle-like GP-II zones or/β" but in this case, a single peak is detected unlike the DSC thermogram, where an overlapping of peaks was observed. Finally, the third peak (Zone III) can be associated to the formation of rod-like β'-phase. The photoacoustic spectrum was measured up to 300°C, for this reason the peak related to the formation of plate-shaped β-phase (Mg_2Si) was not detected.

CONCLUSIONS

The cold-worked and 200°C aged sample showed the highest resilience energy of 12.46 kJ/m³, with a toughness of 11.18 kJ/m³. The samples treated at 150°C, showed the highest plasticity and toughness values, with 58.29 and 56.95 kJ/m³, respectively. On the other hand, the photoacoustic results corroborated the existence of microstructural changes, correlating well with the phase transformations detected using DSC thermograms. The formation of vacancy-silicon clusters was associated to the first peak in the photoacoustic signal. The second peak was related to the formation of GP-I zones and needle-like GP-II zones (β"). The formation of rod-like β'-phase was related to the third photoacoustic signal peak. The photoacoustic analyses proved to be rather useful when measuring the microstructural changes in Al alloys. It is worth mentioning that this technique has not been extensively used in Al alloys for phase transformation determination as a function of temperature.

REFERENCES

1. S. Murtha, *New 6XXX Aluminum Alloy for Automotive Body Sheet Applications: SAE Technical Paper 950718* (SAE Int., Warrendale, PA, 1995).

2. A. Polat, M. Avsar, and F. Ozturk, "Effects of the artificial-aging temperature and time on the mechanical properties and springback behavior of AA6061," Mater. Technol. **49**, 487−493 (2015).

3. C. Bohórquez, M. Sierra Cetina, and J. Lemus, "Influencia del tratamiento térmico de envejecimiento en las propiedades mecánicas de los aluminios 6061 T6 y 6063 T5," Av. Invest. Ing. **13**, 6−11 (2011). https://doi.org/10.18041/1794-4953/avances.1.341

4. Z. Liang and Q. Zhang, "Microstructure and mechanical properties of A356 aluminum alloy prepared by casting combined with back extrusion," Phys. Met. Metallogr. **121** (2), 164−172 (2020).

5. D. Maisonnette, M. Suery, D. Nelias, P. Chaudet, and T. Epicier, "Effects of heat treatments on the microstructure and mechanical properties of a 6061 aluminum alloy," Mater. Sci. Eng., A **28**, 2718−2724 (2015).

6. Y. Huang, L. Liu, Z. Xiao, and S. Wang, "Hot deformation behavior of 6063 aluminum alloy studied using processing maps and microstructural analysis," Phys. Met. Metallogr. **120** (11), 1115−1125 (2019).

7. H. Demir and S. Gündüz, "The effects of aging on machinability of 6061 aluminum alloy," Mater. Des. **30**, 1480−1483 (2009).

8. C. F. Tan and M. R. Said, "Effect of hardness test on precipitation hardening aluminum alloy 6061-T6," Chiang Mai J. Sci. **36**, 276−286 (2009).

9. I. G. Brodova, I. G. Shirinkina, D. Yu. Rasposienko, and T. K. Akopyan, "Structural evolution in the quenched Al−Zn−Mg−Fe−Ni alloy during severe plastic deformation and annealing," Phys. Met. Metallogr. **121** (9), 899−905 (2020).

10. M. Mansourinejad and B. Mirzakhani, "Influence of sequence of cold working and aging treatment on mechanical behavior of 6061 aluminum alloy," Trans. Nonferrous Met. Soc. China **22** (9), 2072−2079 (2012).

11. A. Bedoya, F. Gordillo-Delgado, Y. E. Cruz-Santillana, J. Plazas, and E. Marin, "Thermal effusivity measurement of conventional and organic coffee oils via photopyroelectric technique," Food Res. Int. **102**, 419−424 (2017).

12. K. M. B. Enríquez, MSc Thesis (Universidad Nacional Autónoma de México, Mexico, 2007).

13. E. Marin, "Escuchando la luz: breve historia y aplicaciones del efecto fotoacústico," Lat. Am. J. Phys. Educ. **2** (2), 209−215 (2008).

14. A. Huanosta-Tera, R. Castañeda-Guzmán, and J. L. Pineda-Flores, "Characterization of $Bi_{4−x}R_xTi_3O_{12}$ (R_x = Pr, Nd, Gd, Dy, x = 0.8) layered electroceramics by a photoacoustic method," Mater. Res. Bull. **38**, 1073−1079 (2003).

15. J. M. Pineda Flores, L. Castañeda-Guzmán, and M. Villagrán-Muniz, "Ferro-paraelectric transitions in relax or materials studied by a photoacoustic technique," Appl. Phys. **79** (8), 1166−1168 (2001).

16. R. Castañeda-Guzmán, M. Villagrán-Muniz, J. M. Saniger-Blesa, and S. J. Pérez-Ruiz, "Photoacoustic analysis of the ferroelectric ceramics specific heat," Appl. Phys. **77** (19), 3087−3089 (2000).

17. R. Castaneda-Guzman, M. Villagran-Muniz, and A. Sandoval-Jimenez, "Phase transition on pure and alloy metals by photoacoustic," Proc. SPIE **3572**, 327−330 (1999).

18. R. Castañeda-Guzmán, M. Villagrán-Muniz, and J. M. Saniger-Blesa "Photoacoustic phase transition of the ceramic $BaTiO_3$," Appl. Phys. **73** (5), 623−625 (1998).

19. N. Baddour and A. Mandelis, "The effect of acoustic impedance on subsurface absorber geometry reconstruction using 1D frequency-domain photoacoustics," Photoacoustics **3**, 132−142 (2015).

20. A. G. Bell, "On the production and reproduction of sound by light," Am. J. Sci. **20**, 305−324 (1880).

21. A. G. Bell, Am. J. Sci. **305**, 1880−1910 (1881).

22. D. Schneider and T. Schwarz, "A photoacoustic method for characterizing thin films," Surf. Coat. Technol. **91** (1−2), 136−146 (1997).

23. A. Rosales, R. Castañeda-Guzmán, A. de Ita, C. Sánchez-Aké, and S. J. Pérez-Ruiz, "Detection of zinc blende phase by the pulsed laser photoacoustic technique in ZnO thin films deposited via pulsed laser deposition," Mater. Sci. Semicond. Process. **34**, 93−98 (2015).

24. R. Castañeda Guzmán, M. Villagrán Muñiz, and J. M. Saniger Blesa, "Photoacoustic phase transition of the ceramic $BaTiO_3$," Appl. Phys. **73**, 623−625 (1998).

25. E. Alvarez-Zauco, E. V. Basiuk, R. Castañeda-Guzmán, R. Y. Sato-Berrú, J. M. Saniger-Blesa, M. Villagrán-Muniz, and J. G. Bañuelos, "Phototransformation of C60 thin films by UV pulsed laser irradiation: comparative photoacoustic, AFM, and Raman studies," J. Nanosci. Nanotechnol. **7** (4−5), 1414−1418 (2002).

26. S. Kandpal, "Photoacoustic spectroscopy of thin films of As_2S_3, As_2Se_3 and $GeSe_2$," J. Phys. **69** (481), (2007).

27. A. Pérez-Pacheco, D. R. Acosta-Najarro, R. Castañeda-Guzmán, H. Cruz-Manjarrez, L. Rodriguez-Fernandez, J. C Pineda-Santamaría, and M. Aguilar-Franco, "Evidence of the semiconductor-metal transition in V_2O_5 thin films by the pulsed laser photoacoustic method," J. Appl. Phys. **113**, 184307 (2013).

28. A. Pérez-Pacheco, C. Prieto, R. Castañeda-Guzmán, and J. García-López, "Influence of the growth conditions on the stoichiometry and on the optical properties of titanium oxide thin films prepared by reactive sputtering," Thin Solid Films **517**, 5415−5418 (2009).

29. H. Vargas and L. C. M. Miranda, "Photoacoustic and related photothermal techniques," Phys. Rep. **161** (2), 43−101 (1988).

30. A. Pérez-Pacheco, R. Castañeda-Guzmán, C. Oliva Montes de Oca, A. Esparza-García, and S. J. Pérez Ruiz, "Phase transition of TiO_2 thin films detected by the pulsed laser photoacoustic technique," Appl. Phys. A **102**, 699−704 (2011).

31. *ASTM B308/B308M-10: Standard Specification for Aluminum-Alloy 6061-T6 Standard Structural Profiles* (ASTM Int., West Conshohocken, PA, 2010).

32. B. González Vizcarra, A. Hernández Maldonado, E. Hernández Martínez, and C. Martín del Campo, "Análisis comparativo de las propiedades mecánicas del aluminio 6061-T6 con base a la norma ASTM B 308-10 y fichas técnicas de proveedores locales," Acad. J. Puebla, 779−783 (2016).

33. K. Hajizadeh, S. Ejtemaei, B. Eghbali, and K. J. Kurzydlowski, "Microstructure and mechanical properties of 1050 aluminum after the combined processes of constrained groove pressing and cold rolling," Phys. Met. Metallogr. **121** (1), 72−77 (2020).

34. *ASTM E8/E8M-09: Standard Test Methods for Tension Testing of Metallic Materials* (ASTM Int., West Conshohocken, PA, 2017).

35. https://www.bergeng.com/mm5/downloads/wilson/Wilson_Tukon1202_POD_2014.pdf.

36. *ASTM E92-17: Standard Test Method for Vickers Hardness of Metallic Materials* (ASTM Int., West Conshohocken, PA, 2017).

37. I. Dutta and S. M. Allen, "A calorimetric study of precipitation in commercial aluminum alloy 6061," J. Mater. Sci. Lett. **10**, 323−326 (1991).